

Efficiency of IllustrisTNG in simulating galaxy properties

A good subtitle.

Aurora Grefsrud

Project report



Institute of Physics
NTNU
Norway
December 11, 2020

Abstract

Contents

1	Introduction	3
1.1	Motivation	3
1.2	The structure of this report	4
2	Theory	4
2.1	Galaxy formation	5
2.1.1	Dark matter halos	6
2.1.2	Galaxies	7
2.1.3	Stellar-to-Halo mass relation	9
2.2	Galaxy evolution and classification	11
2.2.1	Elliptical (early type) galaxies	13
2.2.2	Spiral (late type) galaxies	13
2.3	Galaxy properties	15
2.3.1	The Tully-Fisher relation	15
2.3.2	The Faber-Jackson relation and the Fundamental Plane	15
2.3.3	Color bimodality	18
3	Method	18
3.1	IllustrisTNG	18
3.1.1	The simulations	19
3.1.2	Data catalogues	20
3.1.3	Sample reduction	22
3.2	Observational data	22
3.2.1	SAMI Galaxy Survey	23
3.2.2	Other data sets	23
3.3	Morphological classification	24
3.4	Calculating properties	24
3.4.1	Cosmologies and h-dependence	24
3.4.2	Magnitude and colors	25
3.4.3	Stellar mass	26
3.4.4	Size	26
3.4.5	Velocities	27
4	Results and discussions	28

4.1	Stellar to halo mass relation	28
4.2	Tully-Fisher relation	28
4.3	Faber Jackson relation and the fundamental plane	31
4.4	Color bimodality	35
5	Conclusions	36

1 Introduction

1.1 Motivation

The field of astrophysics is a relatively young field of study compared to most other disciplines of science, but in many ways it is the most fundamental. From the tiniest quantum fluctuations at the beginning of time, to the galaxy clusters found at present times, astrophysicists have to cover a range of magnitudes from the smallest particles discovered to the largest structures in the Universe.

In this project galaxies are the focus of study. Theories for how galaxies formed and evolved since the Big Bang have been proposed since they were first discovered, and as new data and new physics emerge, new theories take over for old ones. The model that has been established as the one currently best able to explain observations of the Universe is the Lambda cold dark matter (Λ CDM) model. In this model, the energy in the Universe is made up of about 75 percent dark energy (one theory is that this is the so-called vacuum energy that is pushing the expansion of the Universe), 21 percent dark matter and about 4 percent baryonic (visible) matter (Planck Collaboration et al. 2016).

There are many theories for what dark matter actually is (see e.g., Boveia and Doglioni 2018), but what we do know is that cosmological models require the presence of dark matter to reproduce the structures seen today. Dark matter does not interact with any particles except through gravity. In the Λ CDM model of our Universe, galaxies are located in the center of dark matter halos (hereafter, halos), which extend much further than the actual visible galaxy. Many of the properties of galaxies are linked to its host halo. These, along with several other galaxy properties, are the main focus of this project report.

Hydrodynamical cosmological simulations have been around since the 1980s, starting as N-body simulations of only dark matter particles with a set of initial conditions (Frenk et al. 1983). As computers became more powerful, and physicists learned more about the complicated physics of galaxies, the simulations started to incorporate stars, gas and other baryonic components. The resolution and size of simulations have increased tremendously. Now it is possible to have mass resolutions that show the inner structure of galaxies

and at the same time have a simulation volume that is large enough to be relevant on cosmological scales. In this respect, projects such as the Illustris and EAGLE simulations have pushed the boundaries of modern astrophysics. IllustrisTNG is the new and improved version of the Illustris simulation. The first result-papers were published in 2017, and more data is still being produced. It increases the resolution, size and amounts of physics included, to produce the largest, most detailed simulated Universe to this date.

In this report, the data from the IllustrisTNG simulations will be compared against observational data, to determine whether it manages to reproduce known galaxy properties.

1.2 The structure of this report

Section 2 explains the physics of the main galaxy property relations that are covered in this report. It also contains a glossary with explanation of notation and some astrophysical terms used throughout this report. In section 3, I explain how the simulation and observation data is filtered and converted to the right format for comparison. Section 4 covers the actual comparison of the data, while the section 5 sums up what was learned from the project and looks to the future for what should be studied next.

2 Theory

Some astrophysical notation, terms and constants:

- z - Redshift, a dimensionless measure of time where $z = 0$ denotes the current time and $z \rightarrow \infty$ as we move back in time towards the beginning of the Universe. The redshift also gives the actual physical frequency shift of light emitted from a source moving away from us in an expanding Universe.
- H_0 - The Hubble constant at present time $H(z = 0)$, a cosmological constant related to the expansion rate of the Universe. The best measurements of today sets the value of H_0 to 67.8 km/s/Mpc (Planck Collaboration et al. 2016). Specifically, this means that at $z = 0$ a galaxy located 100 Mpc away is receding from us at a velocity of 67.8 km/s because of the expansion of the Universe.

- h - The “little hubble constant”, given by $H_0 = 100 h$ km/s/Mpc. See section 3.4.1 for further discussion on this.
- G - The gravitational constant.
- M_* - The stellar mass of a given galaxy.
- M_{halo} - The dark matter halo mass of a given galaxy.
- M_\odot - Solar mass. In astrophysics, masses are always given in units of solar masses.
- L - Luminosity. The luminosity of a galaxy is a measure of its total radiated electromagnetic energy per unit time. The absolute magnitude (\mathcal{M}) is related to the luminosity as $\mathcal{M} = -2.5 \log(L/L_\odot) + \mathcal{M}_\odot$.
- R_e - Effective radius. The radius within which half the luminosity of a galaxy is emitted.

2.1 Galaxy formation

Our understanding of the formation and evolution of the Universe as a whole is based on the cosmological principle, which states that matter is distributed spatially isotropically and homogeneously across the Universe on large scales. Of course, we would not have any structure formation if the matter was actually perfectly uniformly distributed in the very beginning of the Universe. It is not completely clear how this initial deviation from homogeneity originated, but at very early times after the Big Bang, the Universe was so small that quantum effects would have played a significant role. These tiny quantum fluctuations may then have been responsible for the initial structure formation we can observe today. Given that these initial density fluctuations in matter were present, gravitational effects will then amplify the overdense regions of space as matter is pulled together. If the Universe did not expand, these instabilities in the density field would just keep growing. However, we know the Universe is expanding, and so the effect is damped significantly. As matter keeps being pulled in over time, the overdense region might reach a “turn-around size” where the gravitational pull is large enough to compensate for the expansion rate of space. Then the matter will collapse towards the center. The exact process for collapse is beyond the scope of this report, but it depends on the ratio of dark matter to baryonic matter, and the properties of the dark matter itself.

2.1.1 Dark matter halos

Dark matter halos are the result of such initial overdense regions of dark matter particles. Halos cover a huge range in magnitude of mass lower than $10^9 M_\odot$ up to sizes of at least $10^{15} M_\odot$. In general, halos are ellipsoid in shape. The spherically averaged density profile of halos, as predicted by N-body simulations of dark matter in a Λ CDM Universe, is well described by the Navarro-Frank-White profile (Navarro et al. 1996). This profile gives us a halo density that is proportional to r^{-1} for smaller radii and r^{-2} for large radii,

$$\frac{\rho}{\rho_{crit}} = \frac{\delta_c}{(r/r_s)(1+r/r_s)^2}, \quad (1)$$

where $\rho_{crit} = 3H_0^2/8\pi G$ is the critical density of the Universe, δ_c is the characteristic overdensity and r_s is the scale radius where the slope changes from r^{-1} to r^{-2} . Both δ_c and r_s may vary for each halo.

Halos grow hierarchically through mergers of smaller halos into larger halos. A smaller halo that merges with a larger halo may survive as a separate entity within the host halo and is then known as a subhalo.

One of the most interesting properties of a Λ CDM Universe is the halo mass function, the number density of halos as a function of their mass. In 1974 the halo mass function was defined by William H. Press and Paul Schechter as:

$$\frac{dn}{dM} = f(\sigma) \frac{\bar{\rho}}{M^2} \frac{d\log(\sigma^{-1})}{d\log(M)}. \quad (2)$$

Where $\sigma = \sigma(R)$ is the variance of the field with a smoothing radius R , $\bar{\rho}$ is the mean density of the Universe and $f(\sigma)$ is the multiplicity function (Press and Schechter 1974). For that work, $f(\sigma)$ was found to be

$$f(\sigma) = \frac{2}{\pi} \sigma \exp(-\sigma^2/2), \quad (3)$$

but other models will give a different multiplicity function.

As an example, Figure 1 shows the halo mass function found by Tinker et al. (2008). In this work, they calculated the halo mass function at $z = 0$ based

on a set of cosmological simulations covering a wide range of box lengths (colored points). The solid black lines show the fit to the Schechter function for three different values of Δ , where Δ is the overdensity within a radius R_Δ with respect to ρ_{crit} .

We will not cover the mathematical details of this analytical solution to the mass function, but it is based on the assumption of spherical collapse and depends on both cosmology and redshift. Until the end of the century, numerical simulations tended to agree with the results presented by Press and Schechter. However, newer and more complex numerical solutions have shown that the Press-Schechter formalism tends to overestimate the amount of smaller halos, while underpredicting the abundance of larger halos.

2.1.2 Galaxies

Dark matter halos formed before baryonic matter could gather in densities even close to that needed to form stars, as there is 6-7 times more dark matter than baryonic matter. The dark matter halos created a gravitational potential well which gave room for the primordial baryonic matter (ionized hydrogen gas) to start collapsing.

As the density of the gas increases, temperature increases and halts the collapse, but through several radiation cooling processes the gas is able to collapse enough for fusion to start and stars to be born. Because of the halos role as initial potential wells, the baryonic matter collapses in such a way that it forms a spinning disk around the center of the halo. This is the birth process of galaxies.

Galaxies are mainly composed of stars and hot gas, with a smaller contribution of stellar remnants, cold gas and dust. Hot gas is hydrogen gas that is fully ionized, and does not collapse into stars, while cold gas has a much lower temperature and can contribute to star formation. There are at least two trillion galaxies in the observable Universe (Conselice et al. 2016), with stellar masses ranging from less than $10^6 M_\odot$ to $10^{12} M_\odot$ and larger.

It has been found that a large fraction of galaxies are gravitationally bound to each other in groups and clusters. Galaxy clusters are the largest gravitationally bound systems in the Universe, and can span a distance of several megaparsecs. They typically contain more than a hundred galaxies, as well as large amounts of intergalactic gas. Galaxies in clusters serve an impor-

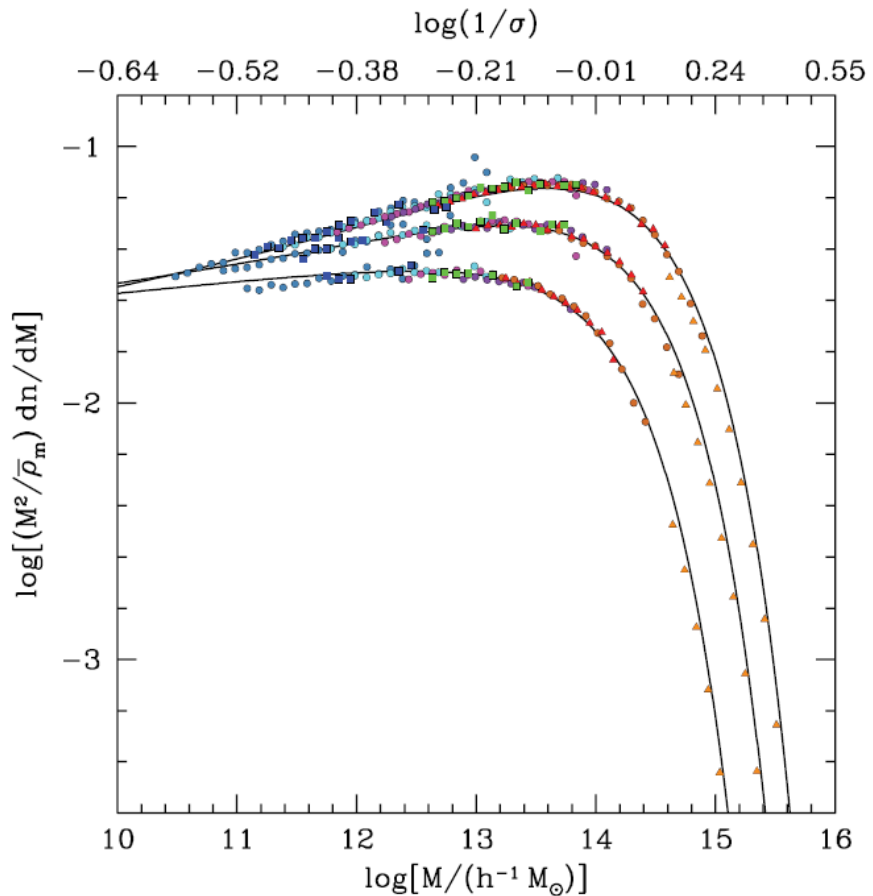


Figure 1: Halo mass function for different overdensities, Δ (points). The color of the points represent the different simulations used to measure the halo mass function. The solid black lines are best fits for each value of the overdensity Δ . They are all three Schechter functions, with varying multiplicity functions to get the best fit to their respective data points. Credit Tinker et al. (2008).

tant purpose to astrophysicists, as they essentially function as tracers of the largest halos in the Universe.

The Λ CDM model for our Universe gives a bottom-up solution to galaxy formation, a hierarchical formation. Essentially this means that larger galaxies have formed through mergers of smaller galaxies. When a galaxy forms, the angular momentum of its initial components get transferred to the galaxy as a whole, and the result is a rotating disk galaxy. Galaxies that are not pure disk galaxies, but have an elliptical component of stars and gas with pressure dominated random motions and which extends in all directions from the center, are results of the merging of galaxies. As many galaxies exist in clusters, the likelihood of a galaxy merger is higher than one might otherwise expect in those regions, and so galaxy clusters contain more elliptical galaxies.

A very important property of the galaxy population is the galaxy luminosity function, which gives the number density of galaxies as a function of their luminosity. The luminosity of a galaxy is directly proportional to its stellar mass, so the luminosity function also gives us the mass distribution of galaxies. Mathematically, the luminosity function is defined as $\phi(L)dL$, where $\phi(L)dL$ is the number density of galaxies in the luminosity range $L \pm dL/2$. In 1976 Paul Schechter proposed a fit to the luminosity function of galaxies on the form

$$\phi(L)dL = \phi^*(L/L^*)^\alpha \exp(-L/L^*)dL/L^*, \quad (4)$$

where ϕ^* is a normalization, L^* is the characteristic luminosity for that sample of galaxies (it will differ for instance for galaxies within a cluster compared to isolated galaxies) and α is the slope of the power law where $L \ll L^*$ (P. Schechter 1976). Figure 2 shows the luminosity function (points) as well as the best fit for equation 4 (solid line). This Schechter function is still a good fit to this day, and is in excellent agreement for galaxies with $L \gg L^*$. For the low mass range of galaxies, the parameter α must be found, and this is one of the challenges of astrophysicists that study galaxy properties.

2.1.3 Stellar-to-Halo mass relation

The stellar-to-halo mass relation (hereafter, SHM relation) gives the stellar mass of a galaxy as a function of its host halo mass. This is particularly

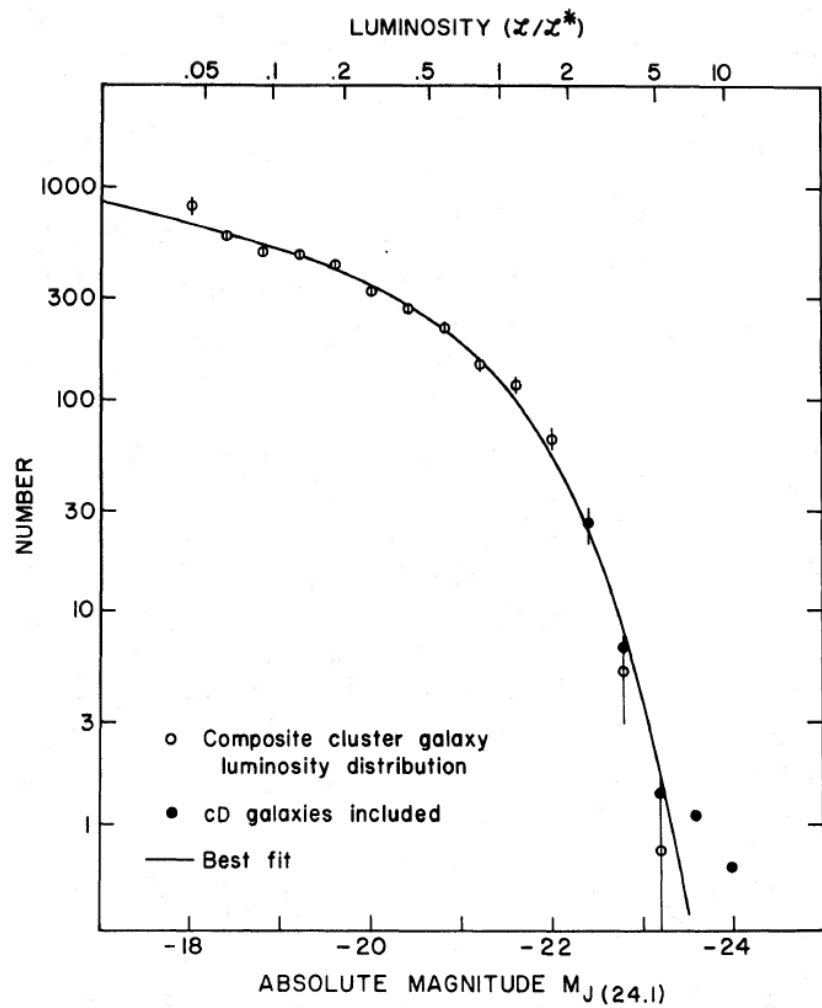


Figure 2: The luminosity function at redshift 0. The open circles correspond to observed galaxies in clusters, while the filled in circles denote cD galaxies (giant ellipticals). The solid line shows the best fit using equation 4. Credit: P. Schechter (1976).

difficult to determine empirically, as it is not possible to directly measure the dark matter halo mass.

One way of looking for this relation is through a method called abundance matching. In abundance matching, the numerically found halo mass function and the observationally found luminosity function are combined. This is done using the simple assumption that the largest halo contains the largest galaxy, the second largest halo contains the second largest halo and so on. By mapping each galaxy to its corresponding halo in such a fashion, the shape of the SHM relation can be found directly.

Using abundance matching, the SHM relation has been found to be well described by a power law with different slopes for the low-mass and high-mass end of the spectrum (Behroozi et al. 2013).

Other ways of studying the SHM relation could be through simulations which include halo and stellar mass like IllustrisTNG, or inferring the halo mass empirically by using the rotational curves of disk galaxies (see section 2.2.2).

2.2 Galaxy evolution and classification

As soon as telescopes became good enough to clearly make out galaxies in the sky, it became apparent to astronomers that galaxies come in many different shapes and sizes. The morphology of the galaxy is closely linked to other properties of the galaxy and is therefore important for the classification of galaxies. Edwin Hubble classified galaxies on a spectra (Hubble 1926), with elliptical galaxies (galaxies that have a dominant spheroidal component) on one end of the spectrum and spiral galaxies (galaxies with a prominent disk component) on the other (Figure 3). The galaxy types were presented as a sequence, so Hubble deemed it convenient to use the adjectives “early” and “late” to describe the two extreme ends of the spectrum. He did consider the fact that these words might be confusing because of their temporal connotations, but went ahead with using “early” and “late” as a proxy for “less complex” and “more complex”, respectively. Indeed this turned out to be confusing, as it is now established that galaxies actually evolve with time along the sequence, starting out as late-type disk galaxies and often ending up as more massive early-type ellipticals.

In the Λ CDM model, galaxies grow through mergers. Mergers are separated into two types, major and minor mergers. Major mergers are events where

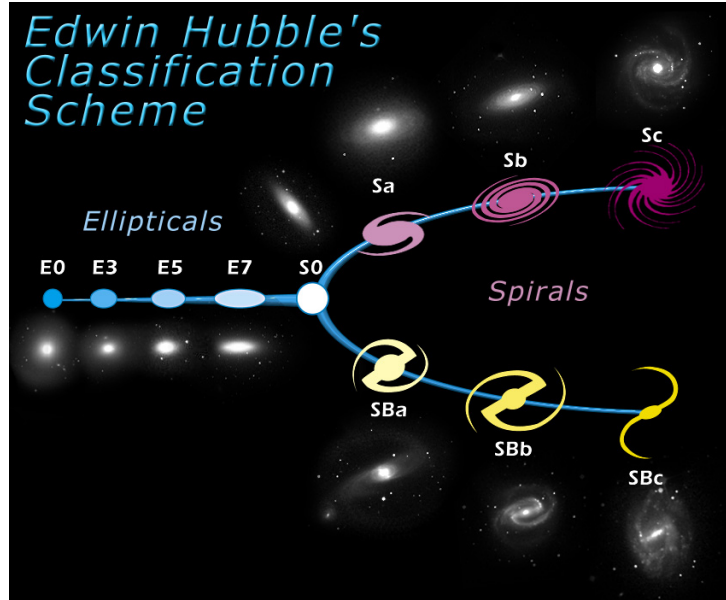


Figure 3: Chart from 1999 showing the original classifications of galaxy morphology. Credit: ESA/Hubble

two galaxies of equal size collide and become one galaxy. Simulations have shown that a major merger between two disk galaxies produces an elliptical. The Milky Way, which is a large spiral galaxy ($M_* > 10^{10} M_\odot$) has probably grown through many smaller minor mergers, and thus kept its disky shape.

It is not always easy to distinguish between a disky elliptical and a spiral with a large spheroidal component (bulge). Some galaxies are also in the middle of a merging process. These can have very irregular shapes, and so are hard to classify. Other galaxies are very small, so called dwarf galaxies. These galaxies tend to have very little stellar mass compared to dark matter, so they do not exhibit the properties of ellipticals, even though they may be more elliptical in shape.

Galaxies were initially separated into the two types (early and late) by their shape, but as astronomers have studied these different galaxy categories, it has become apparent that there are many other properties that also serve to distinguish the two types. Table 1 gives a quick overview of the main properties of early and late type galaxies, while the rest of this section explains them in more detail.

Table 1: Galaxy properties by morphology type

	Early type	Late type
Shape	spheroidal	disk
Color	red	blue
Velocity direction	radial	circular
Stellar population	older	younger
Star formation rate	low	high
Size	smaller	larger
Gas and dust	little	much

2.2.1 Elliptical (early type) galaxies

Elliptical galaxies are mainly pressure-dominated systems, meaning that the motion of the stars is predominantly radial. The largest galaxies in the Universe tend to be ellipticals, but they come in all sizes. The star population of ellipticals is generally older than that of spirals, and there is usually little to no star formation. There is very little gas and dust in ellipticals, and they tend to emit more light in the redder end of the electromagnetic spectrum. Early type galaxies are less common than late type galaxies, and are more usually found in galaxy clusters.

2.2.2 Spiral (late type) galaxies

Late type galaxies have a prominent disk component that orbits around the galaxy's center. The rotational velocity of the disk is typically much larger than the velocity dispersion of the galaxy's bulge. The stars in a spiral galaxy are usually much younger than those in early types. There is a lot of gas and dust present in spirals, giving rise to ongoing star formation. Late type galaxies are bluer in color than early types. Field galaxies, which are not part of any galaxy cluster, are predominantly spirals.

The rotational velocities of the stars at different radii in the disk of spiral galaxies can be measured observationally, and plotting the velocity as a function of radius gives us the velocity curve of the galaxy. If the mass in the galaxy was solely made up of the gas and stars that we are able to detect optically, we would expect the velocity curve to drop off as we get to the outer parts of the galaxy. Assuming the particles move in circular orbits around the center of mass, the circular velocity at a given radius is given by

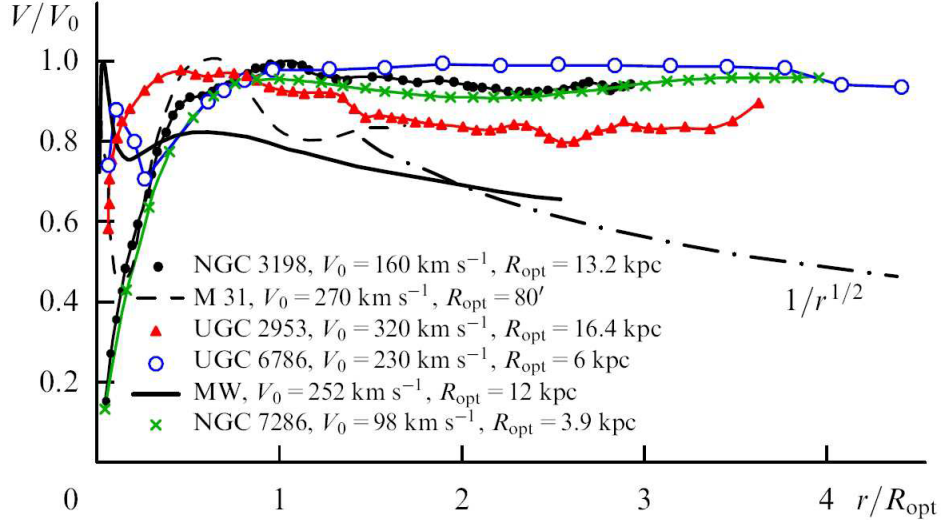


Figure 4: Rotation curves for several spiral galaxies (points). The velocities are normalized with respect to each of the galaxies maximum velocity. Radial distances are in units of the optical radius R_{opt} (the radius within 83% of the light is enclosed). The long-dashed line shows the expected Keplerian curve if there was no dark matter. Credit: Zasov et al. (2017).

the formula

$$v_{circ} = \sqrt{GM(< R)/R}, \quad (5)$$

where $M(< R)$ is the total mass within radius R . However, the observational data shows that the velocity curve does not fall off towards the outer parts of the galaxy, but actually flattens out. An example of this can be seen in Figure 4. There the rotation curves of several spiral galaxies is shown, along with the curve showing the expected fall off of velocity if there was no dark matter (long-dashed line). This perplexed early astrophysicists, as the mass inside the outer radius must be much greater than that which could be accounted for by the stars and gas in the galaxy. An effort to solve this problem led to the theory of dark matter, and later to the Λ CDM model.

2.3 Galaxy properties

In this report I will be looking at many of the main galaxy properties that have been explored throughout the years. We will only be looking at the relations in the present time, $z = 0$, but the relations have been studied across redshifts and many are redshift-dependent.

2.3.1 The Tully-Fisher relation

Tully and Fisher (1977) found a surprisingly good correlation between the luminosity of a spiral galaxy and the characteristic rotational speed of its disk on the form of a simple power law with index α ,

$$L \propto V_{rot}^\alpha. \quad (6)$$

This is known as the Tully-Fisher relation (TFR) (Figure 5). As stellar mass is directly proportional to the luminosity, this gives us the ability to estimate stellar mass from a simple measurement of the rotational velocity.

$$M_* \propto V_{rot}^\alpha \quad (7)$$

α was found to be 3.7 (Tully and Fisher 1977). Later work has found α to lie between 3 and 4 (Lelli et al. 2019; Bloom et al. 2017).

This relation is a great tool for estimating the distance to a galaxy, as the predicted total luminosity can be compared to the apparent magnitude at Earth. For numerical simulations, being able to reproduce the TFR is an essential way to check if the model is reliable.

2.3.2 The Faber-Jackson relation and the Fundamental Plane

At around the same time Faber and Jackson (1976) linked the velocity dispersion and luminosity of early-type galaxies. The proposed relation was on the form of a power law as well,

$$L \propto \sigma^\gamma, \quad (8)$$

with a power law index γ of approximately 4 (Figure 6).

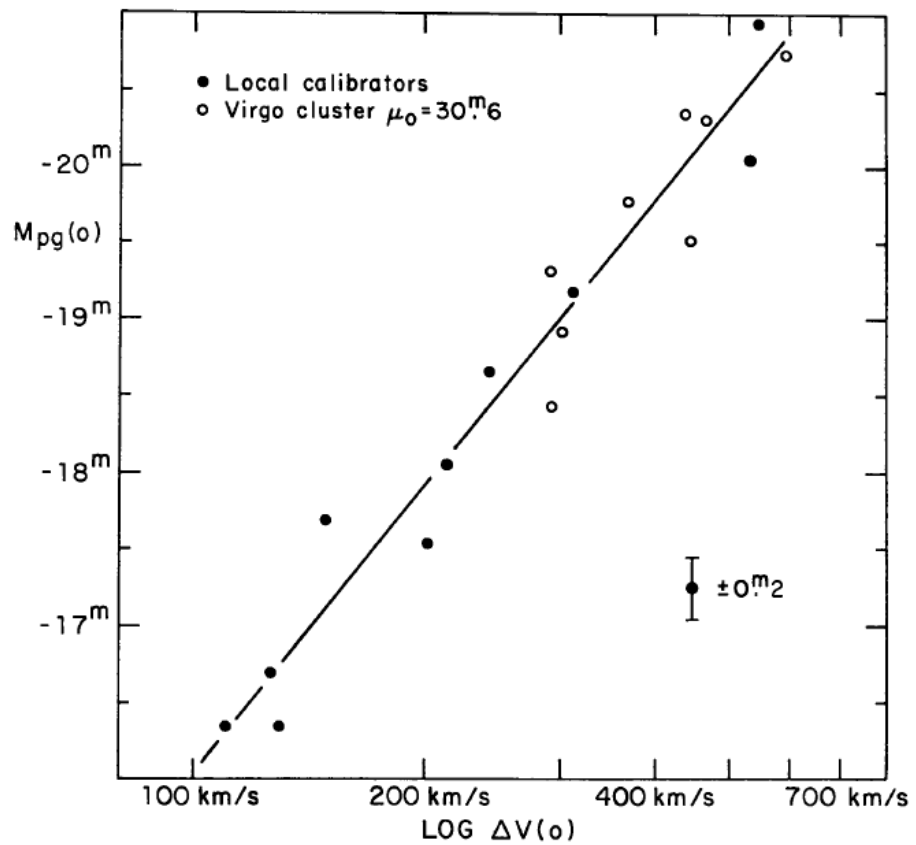


Figure 5: The original figure from the 1977 paper by R.B. Tully and J.R. Fisher, showing the linear fit for the luminosity - velocity values in the log-log plane. Credit: Tully and Fisher (1977)

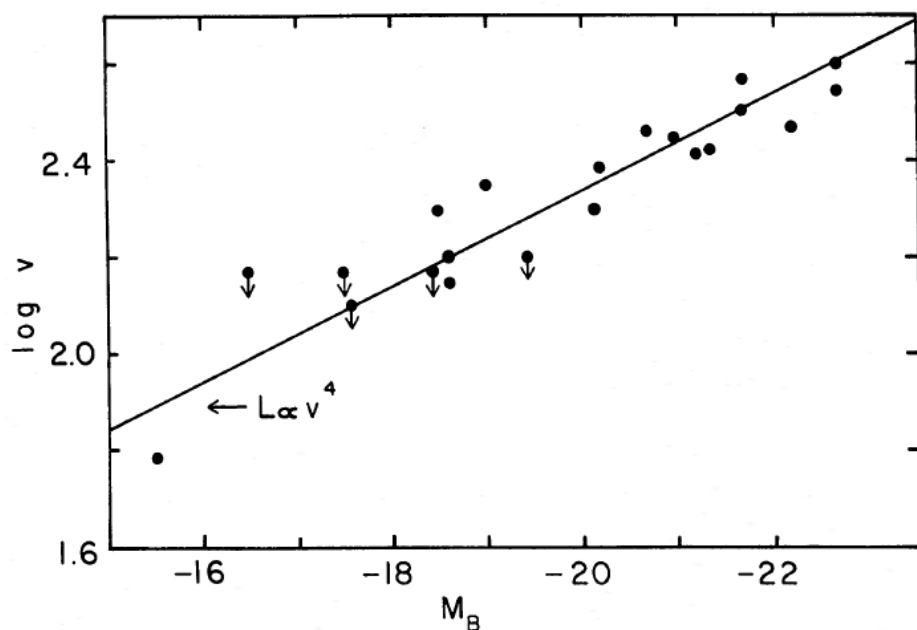


Figure 6: The original fit for the Faber-Jackson relation as presented in the 1976 paper. It shows the velocity dispersion as function of the luminosity in the log-log plane (dots), along with a power law with index 4 (solid black line). Credit: Faber and Jackson (1976)

This is known as the Faber-Jackson (FJ) relation. The scatter in the FJ relation was larger than that found for the TFR however, and it was later found that the velocity dispersion was dependent on the size of the galaxy. This dependence also took the form of a power law, and so the velocity dispersion is more accurately described by the function

$$\sigma \propto L^a R^b. \quad (9)$$

With the radius added into the equation, the scatter became much less significant. Most ellipticals are found on the same plane in σ, R, L space. This plane became known as the Fundamental Plane (FP) (Djorgovski and Davis 1987), and is also something which successful numerical simulations must reproduce.

2.3.3 Color bimodality

Color, in astrophysics, is defined as the difference in magnitudes measured for a galaxy by two different optical filters. A galaxy that is "blue" has a larger amount of blue light than red. In general, galaxies are found to inhabit one of two groups on a color-mass diagram, blue and red (see Figure 7). The blue galaxies are most often late type galaxies, while the red ones are mainly early types. There are many factors that contribute to the color of a galaxy, like stellar age and metallicity as well as the amount of gas the light has passed through and its metallicity.

3 Method

3.1 IllustrisTNG

IllustrisTNG ¹ is the follow-up project after the success of the Illustris simulations (Springel et al. (2017), Pillepich et al. (2017), Naiman et al. (2018), Nelson et al. (2017) and Marinacci et al. (2018)). It is a huge project, built upon a magneto-hydrodynamical cosmological simulation code with added physical processes on a subgrid level (Weinberger et al. 2016). Adding physical processes like gas radiation, star formation, stellar feedback through supernova explosions, supermassive black hole accretion and magnetic fields

¹<https://www.tng-project.org/>

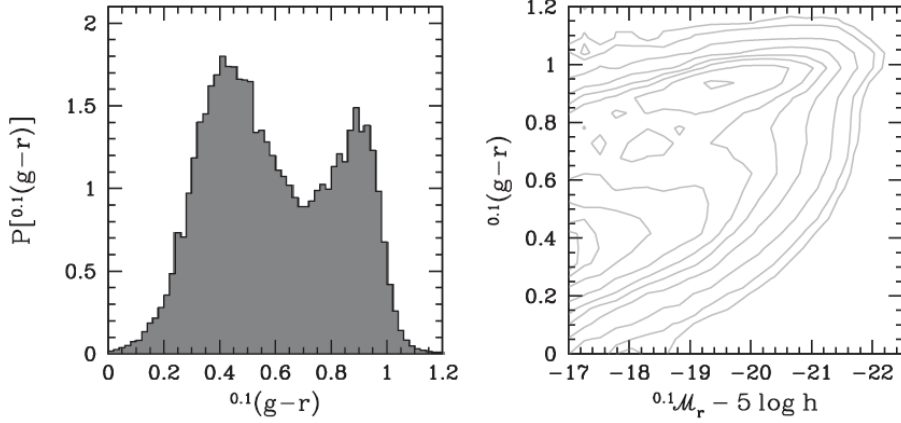


Figure 7: To the left: The probability density of the colors for over 350 000 galaxies in the Sloan Digital Sky Survey. To the right: The color-magnitude relation for the same galaxies, clearly showing two distinct populations. Credit: Mo et al. (2010)

are essential to model galaxy formation and evolution and allows a much better comparison to reality. The data output from the simulations is extensive, and is not meant to be analysed all in one go, but rather through a series of analyses, each targeting a specific scientific question.

3.1.1 The simulations

The IllustrisTNG project includes 18 different simulations with varying resolutions, spatial size and included physics. There are three main simulations, TNG300, TNG100 and TNG50, that differ in volume and resolution. The details of these are summed up in Table 2. Each of the main simulations have been run at three different resolution levels, which makes it possible to study how the outcome is affected by changing only the resolution in a given simulation. TNG100 has a physical box volume of 110.7^3 Mpc^3 , and a baryonic particle resolution of $1.4 \times 10^6 M_\odot$, while the TNG300 simulation has a volume of 302.6^3 Mpc^3 and a baryonic particle resolution of $1.1 \times 10^7 M_\odot$. The TNG50 data is actually not yet available, but it is expected soon, and provides a much higher resolution in a smaller box size. In this project, a large statistical sample of galaxies was needed, as well as detailed structure of the inner part of the galaxies to calculate the different properties, so the

Table 2: The simulation details for the three main TNG simulations. N_{DM} is the amount of dark matter particles. m_{DM} and m_{baryon} is the mass of the dark matter and baryonic particles, respectively.

	Volume [Mpc^3]	N_{DM}	$m_{DM} [M_\odot]$	$m_{baryon} [M_\odot]$
TNG50	51.7^3	2163^3	4.5×10^5	8.5×10^4
TNG100	110.7^3	1820^3	7.5×10^6	1.4×10^6
TNG300	302.6^3	2500^3	5.9×10^7	1.1×10^7

TNG100 simulation was the best choice with respect to size and resolution. The TNG100-1 simulation data, which is the highest available resolution for TNG100, has been used throughout the project and will from now on be referenced as TNG only. A visual representation of parts of the simulations can be seen in Figure 8. TNG uses the results from the Planck Collaboration for its cosmology parameters, $\Omega_{\Lambda,0} = 0.6911$, $\Omega_{m,0} = 0.3089$, $\Omega_{b,0} = 0.0486$, $\sigma_8 = 0.8159$, $n_s = 0.9667$ and $h = 0.6774$ (Planck Collaboration et al. 2016). See section 3.4.1 for more details.

3.1.2 Data catalogues

All the Illustris-TNG data is publically available online at the TNG webpage². The data products that are available for each simulation are snapshots, group catalogs and merger trees as well as some supplementary data sets. There are five different particle types in the simulations, and each has its properties stored as particle fields. These fields include information like position, kinematic data and atomic/chemical composition. For each different run of the simulation, 100 snapshots are created, which are taken at specific redshifts. They include all the particles in the whole volume of the simulation, with 20 of them including all the fields for each particle as well.

The group catalogs provide a convenient way to quickly access already calculated properties of the different halos and subhalos instead of dealing with all the particles in a snapshot. This saves a lot of time and effort, but gives the user less control over what can be analysed. In future work, it might be interesting to do the calculations directly from the snapshots myself. There is one group catalog for each snapshot, and this includes two types of objects, Friends-of-Friends (FoF) and Subfind. The FoF catalog contains all the ha-

²<https://www.tng-project.org/data/>

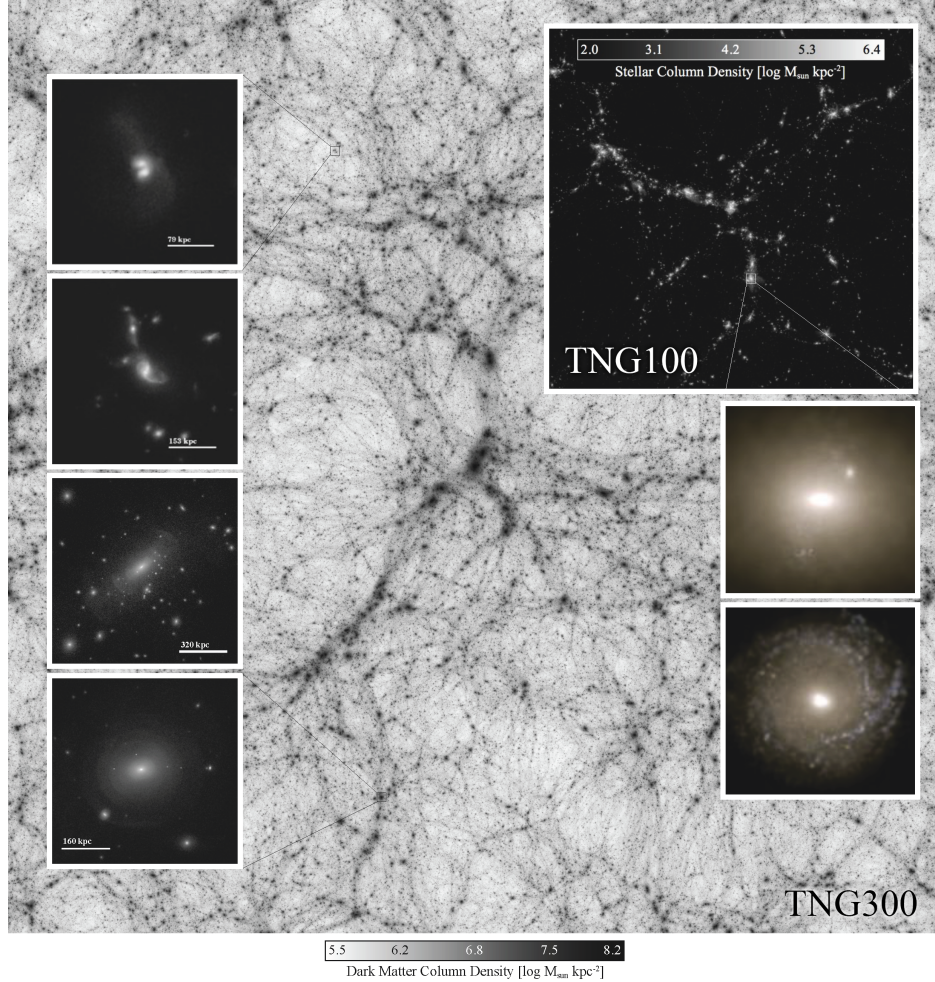


Figure 8: A composite image that illustrates the two simulations TNG100 and TNG300. In the background is the dark matter distribution for the whole TNG300 volume. In the upper right is the stellar mass distribution across the entire TNG100 volume. The panels on the left show galaxy-galaxy interactions, while the panels on the right show the stellar light projections of two $z = 0$ galaxies. Credit: TNG Collaboration

los, and the Subfind catalog contains all the subhalos and their associated galaxy (if there is any) for each halo. Each subhalo has a parent halo, and the largest subhalo in each halo is the central subhalo. The merger trees data products contain the merger history of each subhalo.

This project makes use of the group catalogs for the $z = 0$ snapshot, as we want to compare the output data to observations of the local (present time) Universe.

3.1.3 Sample reduction

The TNG documentation recommends filtering out all subhalos that are flagged with the *SubhaloFlag* field, and so these were cut from the data. These are most probably subhalos of non-cosmological origin, and so should not be considered real galaxies.

For the relations covered in this project, it is desirable to use only the central galaxies in each halo. This is because satellite galaxies are more affected by their environment, which in turn affects the kinematic and structural properties of the galaxy. This will naturally lead to a scatter in the galaxy scaling relations that are being studied, which central galaxies will not display. The FoF catalog contains the index for the largest subhalo in each halo, so combining this information with the Subfind catalog allows one to create a subset of the data that contains only the central galaxies.

Only galaxies with stellar mass greater than $10^9 M_\odot$ are used, which corresponds to about 700 stellar particles. Galaxies with fewer particles have less reliably resolved inner structure, and so they are not taken into account for this study.

3.2 Observational data

When possible, it is good practice to use the same observational data for comparisons with the simulation data. Trying to accomplish this, in this work I used the SAMI Galaxy Survey (Bryant et al. 2015). For the SHM relation however, it was not possible to use the SAMI data set, so other works have been chosen to use for that comparison. All the data sets and best fits used in comparing the results from TNG to observations are described in this section.

3.2.1 SAMI Galaxy Survey

The Sydney – Australian Astronomical Observatory Multi-Object Integral Field Spectrograph (SAMI) is mounted on the Anglo-Saxon telescope in Australia. The SAMI Galaxy Survey³ is a spectroscopic survey of a large sample of galaxies in the nearby Universe ($z < 0.113$). The survey was started in 2013, and ended in 2018. There have been two major data releases, with the newest being Data Release Two (DR2) (Scott et al. 2018). DR2 includes data for 1559 galaxies, which is about 50 % of the full galaxy survey. The data products available are IFS data cubes and 2D maps, as well as catalogue data. As the same galaxies have been cataloged in several other studies, data products from those studies are added to SAMI data. Analysing data cubes and 2D maps falls outside the scope of this work, so catalogue data with some properties already estimated is used where possible.

3.2.2 Other data sets

For the SHM relation, best fit models from two different abundance method papers were used in the comparison to TNG.

The first one found a fit to the data by using a power law for the high mass end, and a subpower law for the low mass end (Behroozi et al. 2013).

$$\log(M_*(M_{halo})) = \log(\epsilon M_1) + f(\log(M_{halo}/M_1)) - f(0), \quad (10)$$

$$f(x) = -\log(10^{\alpha x} + 1) + \delta \frac{(\log(1 + \exp(x)))^\gamma}{1 + \exp(10^{-x})}.$$

Here M_1 is a characteristic halo mass, δ is the strength of the subpower law, α is the power law slope for $M_{halo} \ll M_1$ and γ is the power law index for $M_{halo} \gg M_1$. The best fit values for the parameters are $M_1 = 11.514 \pm (0.053, 0.009)$, $\delta = 3.508 \pm (0.087, -0.369)$, $\alpha = -1.412 \pm (0.020, -0.105)$, $\epsilon = -1.777 \pm (0.133, 0.146)$ and $\gamma = 0.316 \pm (0.076, -0.012)$.

The second one employed the same function for the fit as Behroozi et al. (2013), but with different data. The best fit parameters were found to be $M_1 = 11.632 \pm (0.008, 0.009)$, $\delta = 3.797 \pm (0.026, 0.021)$, $\alpha = -2.352 \pm (0.026, -0.021)$, $\epsilon = -1.785 \pm (0.010, 0.008)$ and $\gamma = 0.600 \pm (0.10, 0.013)$ (Zanisi et al. 2019).

³<https://sami-survey.org/>

3.3 Morphological classification

As several of the relations studied in this project relate to the morphological type of the galaxies, it was necessary to filter out early and late type galaxies to study separately. This can be done in different ways. In many studies of TNG, several criteria for classification have been employed at the same time like star formation rate, luminosity profiles, gas fraction and visual classification (see e.g. Lu et al. (2020) and Genel et al. (2017)). In this work, the fraction of gas inside the effective radius of each galaxy has been chosen as the single criteria for classification,

$$f = M_{\text{gas}}/M_{*}. \quad (11)$$

For $f > 0.1$, the galaxy is classified as late type, while for $f < 0.1$, the galaxy is classified as early type. Including a criteria for star formation rate did not significantly change the outcome, so it was determined to keep the selection process simple.

In the SAMI DR2, the galaxy morphology is determined visually. They are classified into four different categories: E, S0, Sa/Sb and Sc/Sd/irregulars, as well as intermediate categories if the galaxy is hard to place. See Figure 3 in section 2.2 for a visualisation of the different galaxy classifications. In this analysis, the E and S0 are considered early type, while Sa/Sb and Sc/Sd/irregulars are considered late types.

3.4 Calculating properties

3.4.1 Cosmologies and h-dependence

When making measurements of galaxy properties, some assumptions about the underlying cosmology of the Universe must be made. One of these assumptions is the value of the Hubble constant H_0 , more commonly represented by h , where $H_0 = 100h$ km/s/Mpc. In addition to several other cosmological parameters, this constant is used when running a cosmological simulation. Astrophysical properties, both numerical and observational, are presented in publications with an h-dependence (leaving the user to specify the cosmology) or without an h-dependence (by assuming a value for h).

For IllustrisTNG, $h = 0.6774$ and the explicit h -dependence of each property

Table 3: The h -dependence and units for the galaxy properties used in this work. For TNG, the dependency is given in the data documentation. The dependencies for SAMI are the standard dependencies for observational data, as found in Table 2 in Croton (2013).

	TNG	SAMI
Stellar mass	$M_{\odot}h^{-1}$	$M_{\odot}h^{-2}$
Halo mass	$M_{\odot}h^{-1}$	-
Size	$\text{kpc } h^{-1}$	$\text{kpc } h^{-1}$
Luminosity	mag	mag +5 log(h)
Velocity	km/s	km/s

value is stated clearly in the documentation. For the SAMI data catalogue, no h -dependence is explicitly stated in the documentation or data release papers, but the Hubble constant used is given as $h = 0.7$.

Best practice dictates that to compare works with different assumed Hubble constants, the h used in those specific works should be replaced with the most recent value for h (Croton 2013). The values for galaxy properties will then be comparable. In Table 3 the h -dependency of the galaxy properties of TNG as well as the common h -dependencies for observational data is shown along with their corresponding units. In this work, all data results are converted to the TNG cosmology, which uses the newest values for the cosmological parameters.

3.4.2 Magnitude and colors

The magnitude (\mathcal{M}) is a measure of the total luminosity (L) of the galaxy such that $\mathcal{M} = -2.5 \log(L/L_{\odot}) + \mathcal{M}_{\odot}$, where L_{\odot} is the solar luminosity and \mathcal{M}_{\odot} is the solar magnitude.

For the TNG data, the Subhalo field `SubhaloStellarPhotometrics` is used to get the magnitudes based on the summed up luminosities of all the stellar particles in the Subhalo. Eight bands are available, but in this work only the g- and i-band are used. The g-i colors are calculated by simply subtracting the i-band magnitude from the g-band magnitude.

In SAMI, g-i color values are adopted from the GAMA Sérsic catalogue (Driver et al. 2011).

3.4.3 Stellar mass

The stellar mass of each galaxy in both TNG and SAMI are readily available in the group catalogs. Stellar mass estimates depend on the stellar initial mass function (IMF), which describe the spectral evolution of a population of stars, and as such the relationship between luminosity and mass in a given spectral band. SAMI and TNG both adopt a Chabrier (2003) IMF.

For SAMI DR2, the stellar mass values are taken from the GAMA Sérsic catalogue (Driver et al. 2011). They calculate the stellar masses by using the i-band magnitude and g-i color of each galaxy through the formula $\log M_*/M_\odot = 1.15 + 0.70(g - i) - 0.4\mathcal{M}_i$, where \mathcal{M}_i is the rest-frame i-band absolute magnitude (Taylor et al. 2011).

3.4.4 Size

In observational data, galaxy sizes are always projected sizes, as they are derived from 2D images. A common measure of the size of a galaxy is the effective radius, which is the radius within which half the light of the galaxy is contained. This quantity depends on the analysis and quality of the 2D profiles, and may not be able to include all the light in a galaxy in the way that we can ensure for computer simulated data. The radius also depends on which optical filter the measurements are made in, as different filters will capture different parts of the galaxy.

For TNG data, the `SubhaloHalfmassRadStellar` field has been used. The half-mass radius is the radius of a spherical volume within which half the stellar mass is found. It is the 3D half-mass radius (R_e), as it is not a projected quantity. This value is generally higher than the 2D half-light radius (r_e) for a given mass up to $M_* < 10^{10.5}$, as seen in Genel et al. (2017). To be consistent with observed data, the 3D radius is projected by using the relation $R_e = \frac{4}{3}r_e$ which generally holds for pressure supported systems like elliptical galaxies (Wolf et al. 2010).

The SAMI catalog data takes the values for the effective radius from the GAMA Sérsic catalogue (Driver et al. 2011). The effective radius is defined as the semi-major axis half-light radius, measured in the r-band. The values are given in units of arcsec which were then converted to a physical radius in kpc.

Then these semi-major axis radii are converted to circular radii using the formula

$$r_{e,circ} = r_{e,sm} \sqrt{(1 - \epsilon)}, \quad (12)$$

where $r_{e,circ}$ is the circular radius, $r_{e,sm}$ is the semi-major axis effective radius and ϵ is the eccentricity.

3.4.5 Velocities

Galaxy velocities are for early and late type galaxies are usually defined as respectively velocity dispersion and rotational velocity. This is because of the shape of the two different galaxy types. It makes more sense to talk about velocity dispersion in a pressure dominated system and rotational velocity in a rotating disk.

For the TFR, rotational velocities are needed. In TNG, the Subhalo field `SubhaloVMax` gives the maximum value for the spherically averaged rotation curve of a given galaxy. As the rotational curves are nearly flat for large enough radii, it should not be very important at which radius the observational rotational velocity is measured, as long as it is in the flat part of the curve. Accordingly, `SubhaloVMax` is used as the rotational velocity for the TNG data.

Rotational velocities were not available as SAMI catalogue data, but an extensive analysis of the 2D velocity maps in DR2 is found in Bloom et al. (2017). They defined the rotational velocity as the velocity at $2.2 R_e$, which should lay well into the flat regime of the velocity curve, and coincide well with the maximum velocity. Their best fit for the TFR was used in our comparison,

$$\log(V_{rot}) = 0.31 \pm 0.0092 \times \log(M_*) - 0.93 \pm 0.1. \quad (13)$$

When talking about the FJ relation and the fundamental plane, velocity dispersion is the velocity measure which is used. The field `SubhaloVelDisp` from the TNG group catalog gives the velocity dispersion of all the member particles for each subhalo. In SAMI catalog data, the given velocity dispersion is averaged within an aperture with radius equal to the effective radius of each galaxy.

4 Results and discussions

The results of the comparison of galaxy property values for TNG and SAMI are presented in this section.

4.1 Stellar to halo mass relation

The SHM relation from TNG is plotted in Figure 9, along with the best fits from Behroozi et al. (2013) and Zanisi et al. (2019). At low halo masses, the TNG galaxies have on average slightly higher stellar masses than Behroozi et al. (2013), but the difference is significant from Zanisi et al. (2019). The turn around point M_1 for TNG is similar to that of both abundance matching fits. For $M_{halo} > 10^{12} M_\odot$, the TNG SHM relation deviates significantly from the abundance matching fit by having a much steeper slope. This indicates a value for γ in equation 10 closer to unity. The more recent results from Zanisi et al. (2019) agrees better with the high mass slope, but the difference is still significant. The deviation from observations is expected, as TNG has been found to produce galaxies with too high stellar mass in larger subhalos (//cite). This might indicate a too high star formation rate in these galaxies.

4.2 Tully-Fisher relation

The TFR for the late type galaxies in TNG is shown in Figure 10 along with the best fit for the SAMI data found in Bloom et al. (2017). The linear fit to TNG gives a slope of 4.13. This is steeper than that found for the SAMI data, which has a slope of 3.23. As massive TNG galaxies were found to have lower halo masses compared to data, this would also lead to lower velocity values, and might explain the difference in slope. Rotational velocities for TNG are chosen as the maximum velocity on the velocity curve, while Bloom et al. (2017). use the velocity at $r = 2.2r_e$. A better comparison could be made by choosing the same definition for the rotational velocity for both data sets. This is something which could be explored in future work.

It might also be interesting to investigate the Baryonic Tully-Fisher relation by adding the hydrogen gas mass and velocity measurements to the stellar measurements.

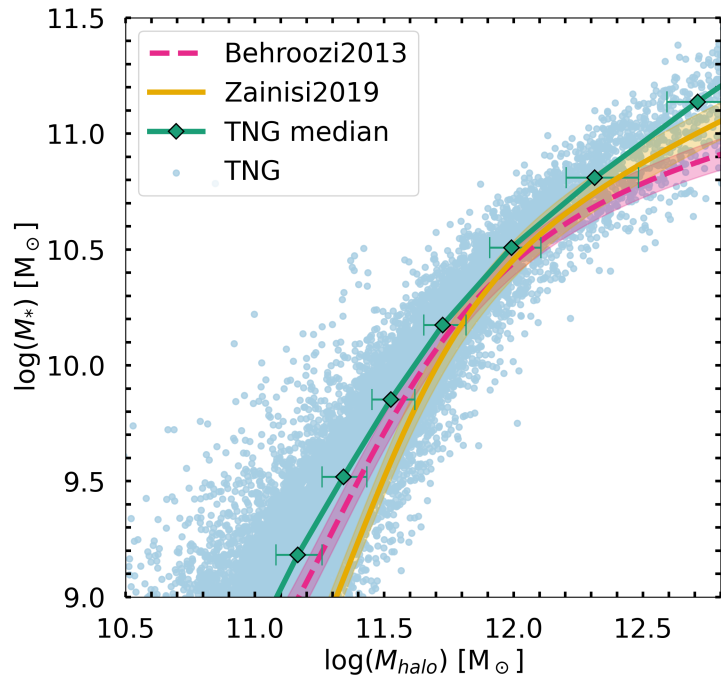


Figure 9: The SHM relation of TNG is shown (blue dots), along with median points (green markers) with error bars showing the 25-75 percentile. The best fit from abundance matching from Behroozi et al. (2013) (pink dashed line) and Zanisi et al. (2019) (yellow line)) are also shown.

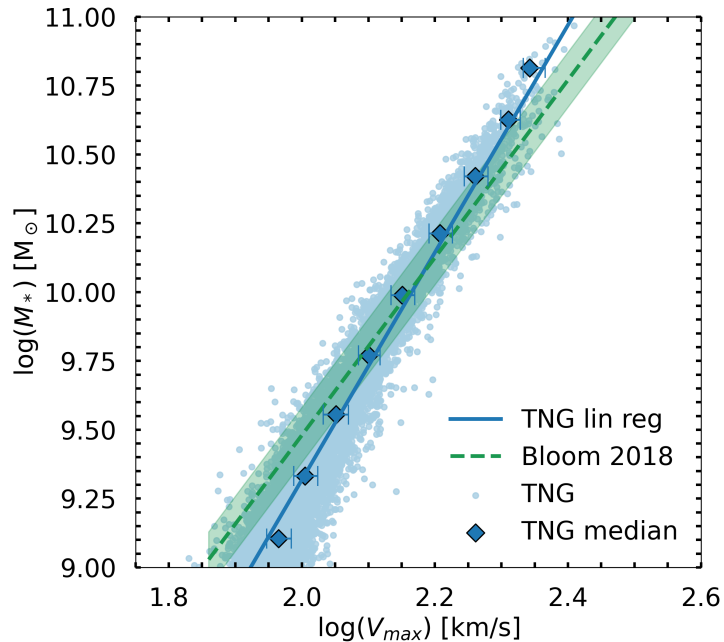


Figure 10: The TFR for TNG (blue dots). The median points for TNG are plotted with error bars, showing the 25-75 percentile. The TNG linear fit is also provided (blue line). The best fit for the SAMI data from Bloom et al. (2017) is also shown (dashed line).

4.3 Faber Jackson relation and the fundamental plane

The velocity dispersion as function of stellar mass (FJ relation) can be seen in Figure 11. The trend for the TNG data is a clear power law as expected. Using linear regression, the slope for TNG was found to be 3.14, with a zero-point of 4.21. Compared to the observational data, the simulation shows lower σ values, by about 0.1-0.2 dex, while the slope is similar. The velocity dispersion in TNG galaxies is averaged across all particles identified by subfind while for SAMI, they are calculated from stars only and just in the inner part of the galaxy. In general, gas has a lower σ than stars and dark matter, so this could push the total σ down for TNG. However, in early-type galaxies there is little gas so the impact would be expected to be small. Other studies have also found that simulations tend to get lower values for σ (Sande et al. 2018), so this might be a limitation of the simulations.

The stellar mass-radius relation is shown in Figure 12. TNG has early type galaxies with smaller radius than SAMI. The radius for TNG is defined as the half mass radius, while SAMI uses half-light radius as described in section 3.4.4. Half-light radius tends to be larger than half-mass radius (Sande et al. 2018). Apart from this, the general trend of the relation is similar in both data sets.

The σ -radius relation can be seen in Figure 13. This relation is also affected by the systematically lower σ values for TNG, as well as the lower radii. The scatter in the data is comparatively large for both TNG and SAMI.

For the mass-radius and σ -radius relations it would be interesting to calculate the half-light radius for TNG instead of using the half-mass radius (this has been done for instance by Genel et al. (2017)). This could be studied in future work, along with choosing the same method of calculating the velocity dispersion for simulation and observation data.

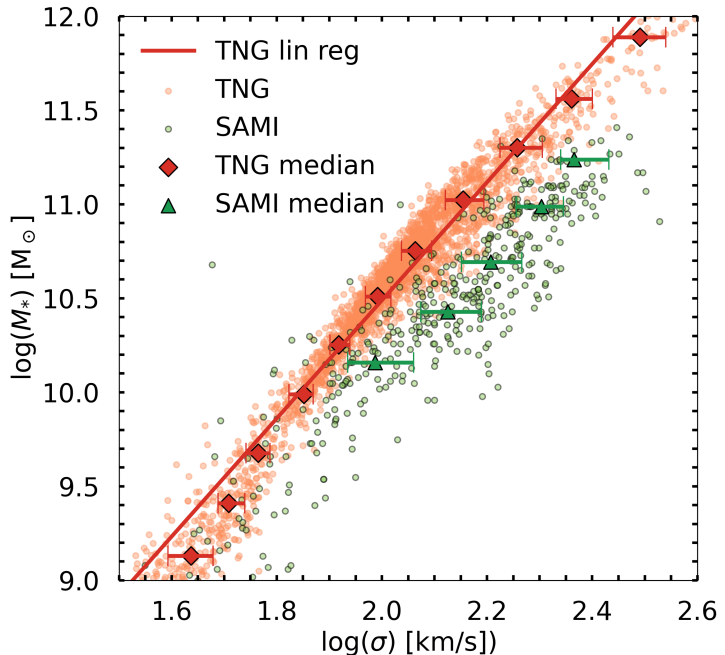


Figure 11: The FJ relation in early type galaxies for TNG (red dots) and SAMI (green dots). The median values with 25-75 percentile error bars are also shown. For SAMI, the median values are not calculated below a stellar mass of $10^{10} M_{\odot}$. The linear fit to the TNG data is shown as a solid red line, and has a slope of 3.14 with a zero-point of 4.2.

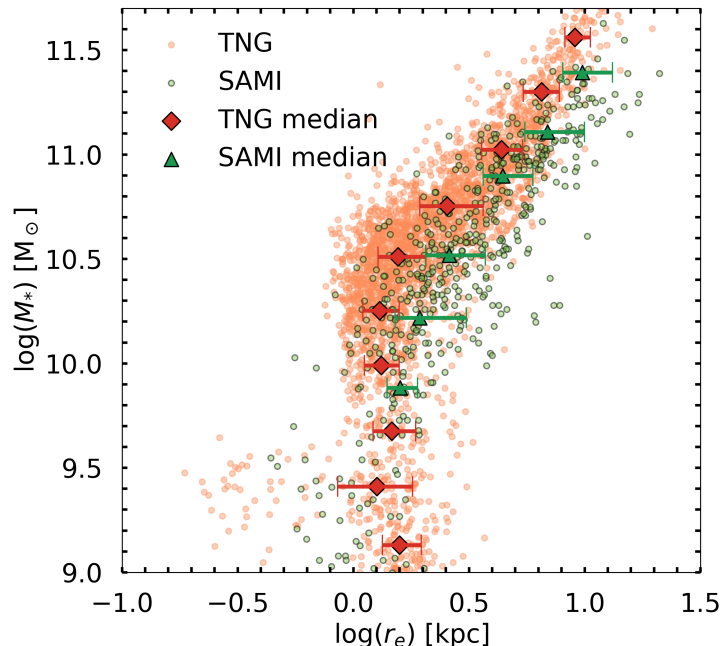


Figure 12: The stellar mass as a function of effective radius in early type galaxies for TNG (red dots) and SAMI (green dots). Median values are also shown with 25-75 percentile error bars. SAMI median values are only calculated for masses above $M_* = 10^{9.7} M_\odot$ as there are too few data points below this mass.

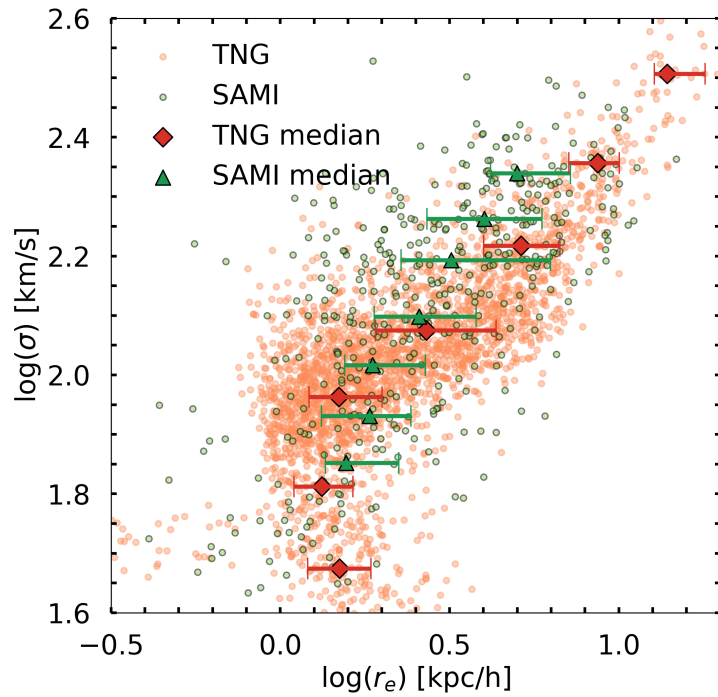


Figure 13: Velocity dispersion as a function of effective radius for early type galaxies for TNG (red dots) and SAMI (green dots). Also included are median values and 25-75 percentile error bars for both data sets.

4.4 Color bimodality

The g-i color-mass diagrams for TNG and SAMI are shown in Figure 14. There is a distinct separation between early and late type galaxies in TNG, as expected. For SAMI, the distinction is less clear. The early type galaxies in SAMI are redder than the late type galaxies on average, but there is a significant amount of late type galaxies with similar mass and color as the early types. Interestingly enough, it has been noted by other work that TNG produces too many red late type galaxies compared to observations (Nelson et al. 2017), but in this case we get the opposite effect. This might have to do with the different classification method of early and late type galaxies in SAMI and TNG. In general, the SAMI galaxies are also on average redder than the TNG galaxies. Nelson et al. (2017) found the color bimodality in TNG to generally be in good agreement with observations despite the larger amount of red late type galaxies, and notes a large improvement with respect to the original Illustris simulation.

In Figure 15 the PDF for the TNG and SAMI g-i colors are shown. The peaks coincide well for the two data sets, but the slight shift towards redder values for SAMI is apparent here also. The SAMI late type galaxy distribution has a peak, but it is not as profound as for TNG. If galaxies with mass down to $10^8 M_\odot$ are included for SAMI, the peak becomes much more profound, so in future work it would be interesting to look at TNG data for galaxies with smaller stellar masses as well. It is worth noting that TNG has a distribution of early type galaxies with an extra “bump” towards the blue end of the spectrum, while SAMI has a bump on the late type galaxy distribution. This is also something which could be studied in further work.

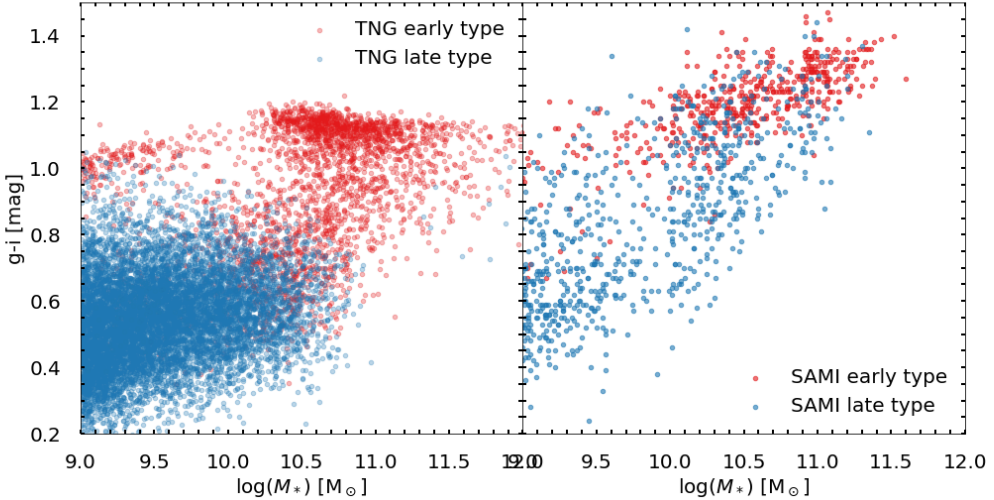


Figure 14: Left: TNG g-i color-mass diagram. Late type and early type galaxies are shown in different colors, blue and red respectively. Right: SAMI g-i color-mass diagram with early type (red) and late type galaxies (blue) plotted separately.

5 Conclusions

A study of the data output from the IllustrisTNG simulation TNG-100 for redshift 0 was carried out to see how well it reproduces known galaxy properties. The properties studied were the stellar to halo mass relation, the Tully-Fisher relation, the Faber-Jackson relation and fundamental plane as well as the galaxy color bimodality. Only galaxies with stellar mass greater than $10^9 M_\odot$ were used in the study, to ensure sufficient resolved structure in the inner parts of the galaxies. All the property values were taken from the publicly available data catalogs. For comparison purposes the observational data from the SAMI galaxy survey were chosen, which also are publicly available as data catalogs.

For the stellar to halo mass relation, TNG produces galaxies with too high stellar mass at both low and high halo masses compared with results from abundance matching. The general trend and characteristic mass is however similar.

The Tully-Fisher relation for TNG has a steeper slope than that found for

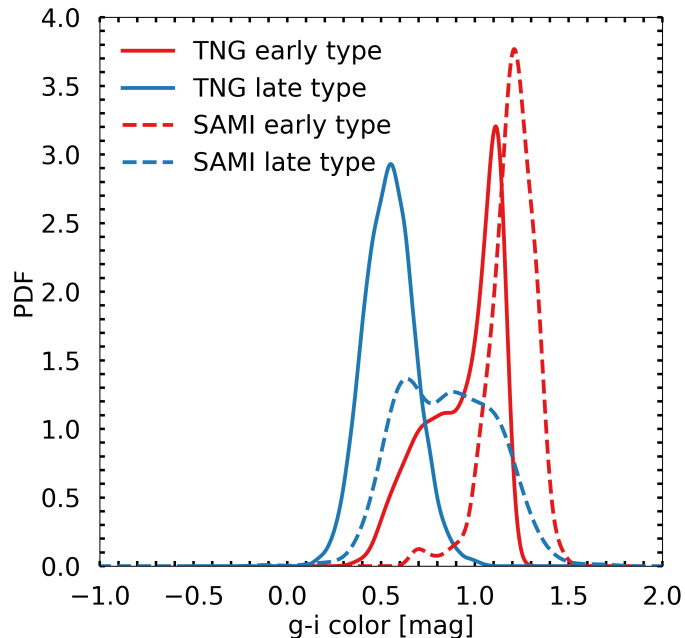


Figure 15: The distribution of g-i color in TNG and SAMI. Kernel density weighted PDF (with Gaussian kernels) are shown for TNG early and late types (red and blue solid lines) as well as for SAMI (red and blue dashed lines). The values are not normalized, so the height of the peak is not comparable, but the x-position and width is.

SAMI. There is however many deficits in the comparison, and further study is required to investigate this.

Looking at early type galaxies, the Faber-Jackson relation for TNG has a similar slope to that of SAMI, but there is a systematic shift towards lower velocity dispersions for the simulation compared to the observed data. This is again something which could be further studied in future work, specifically by calculating the velocity dispersions for TNG only in the inner parts of the galaxies and only using stellar particles. When looking at the other projections of the fundamental plane, the effective radius for TNG is lower than that for SAMI. Here the different definitions of effective radii plays a significant role, and in future work it would be beneficial to try to use the most similar definitions.

The color bimodality of galaxies was also investigated, and it was found that TNG galaxies were on average bluer than SAMI galaxies. However, here the much smaller data sample in SAMI becomes apparent. Again there is also the differing methods of assigning the galaxy morphology types to take into account.

////

In conclusion, IllustrisTNG is a powerful tool for studying galaxy formation and evolution. On most of the properties studied here, it shows excellent agreement to observations. In future works, I would like to study entire snapshots instead of the premade data catalogues. In particular, it would be interesting to look at the velocity profiles of galaxies in more detail. Also, SAMI data release 3 is being released right now. Getting a larger observational sample for comparison would be great.

Cosmological hydrodynamical simulations are getting more and more powerfull as computer power increases and we get a better understanding of the physics that governs the evolution of our universe. There is of course always room for improvements, and so the field of astrophysics will just keep evolving as we learn and grow.

References

- [1] Peter S. Behroozi et al. “The Average Star Formation Histories of Galaxies in Dark Matter Halos from $z = 0\text{--}8$ ”. In: *The Astrophysics*

- cal Journal* 770.1, 57 (June 2013), p. 57. DOI: [10.1088/0004-637X/770/1/57](https://doi.org/10.1088/0004-637X/770/1/57). arXiv: [1207.6105 \[astro-ph.CO\]](https://arxiv.org/abs/1207.6105).
- [2] J. V. Bloom et al. “The SAMI Galaxy Survey: the low-redshift stellar mass Tully–Fisher relation”. In: *Monthly Notices of the Royal Astronomical Society* 472.2 (July 2017), pp. 1809–1824. ISSN: 1365-2966. DOI: [10.1093/mnras/stx1701](https://doi.org/10.1093/mnras/stx1701). URL: <http://dx.doi.org/10.1093/mnras/stx1701>.
- [3] Antonio Boveia and Caterina Doglioni. “Dark Matter Searches at Colliders”. In: *Annual Review of Nuclear and Particle Science* 68.1 (Oct. 2018), pp. 429–459. ISSN: 1545-4134. DOI: [10.1146/annurev-nucl-101917-021008](https://doi.org/10.1146/annurev-nucl-101917-021008). URL: <http://dx.doi.org/10.1146/annurev-nucl-101917-021008>.
- [4] J. J. Bryant et al. “The SAMI Galaxy Survey: instrument specification and target selection”. In: *Monthly Notices of the Royal Astronomical Society* 447.3 (Mar. 2015), pp. 2857–2879. DOI: [10.1093/mnras/stu2635](https://doi.org/10.1093/mnras/stu2635). arXiv: [1407.7335 \[astro-ph.GA\]](https://arxiv.org/abs/1407.7335).
- [5] Gilles Chabrier. “Galactic Stellar and Substellar Initial Mass Function”. In: *Publications of the Astronomical Society of the Pacific* 115.809 (July 2003), pp. 763–795. DOI: [10.1086/376392](https://doi.org/10.1086/376392). arXiv: [astro-ph/0304382 \[astro-ph\]](https://arxiv.org/abs/astro-ph/0304382).
- [6] Christopher J. Conselice et al. “The evolution of galaxy number density at $z < 8$ and its implications”. In: *The Astrophysical Journal* 830.2 (Oct. 2016), p. 83. ISSN: 1538-4357. DOI: [10.3847/0004-637X/830/2/83](https://doi.org/10.3847/0004-637X/830/2/83). URL: <http://dx.doi.org/10.3847/0004-637X/830/2/83>.
- [7] Darren J. Croton. “Damn You, Little h! (Or, Real-World Applications of the Hubble Constant Using Observed and Simulated Data)”. In: *Publications of the Astronomical Society of Australia* 30 (2013). ISSN: 1448-6083. DOI: [10.1017/pasa.2013.31](https://doi.org/10.1017/pasa.2013.31). URL: <http://dx.doi.org/10.1017/pasa.2013.31>.
- [8] S. Djorgovski and Marc Davis. “Fundamental Properties of Elliptical Galaxies”. In: *The Astrophysical Journal* 313 (Feb. 1987), p. 59. DOI: [10.1086/164948](https://doi.org/10.1086/164948).
- [9] S. P. Driver et al. “Galaxy and Mass Assembly (GAMA): survey diagnostics and core data release”. In: *Monthly Notices of the Royal Astronomical Society* 413.2 (May 2011), pp. 971–995. DOI: [10.1111/j.1365-2966.2010.18188.x](https://doi.org/10.1111/j.1365-2966.2010.18188.x). arXiv: [1009.0614 \[astro-ph.CO\]](https://arxiv.org/abs/1009.0614).

- [10] S. M. Faber and R. E. Jackson. “Velocity dispersions and mass-to-light ratios for elliptical galaxies.” In: *The Astrophysical Journal* 204 (Mar. 1976), pp. 668–683. DOI: [10.1086/154215](https://doi.org/10.1086/154215).
- [11] C. S. Frenk et al. “Nonlinear evolution of large-scale structure in the universe”. In: *The Astrophysical Journal* 271 (Aug. 1983), pp. 417–430. DOI: [10.1086/161209](https://doi.org/10.1086/161209).
- [12] Shy Genel et al. “The size evolution of star-forming and quenched galaxies in the IllustrisTNG simulation”. In: *Monthly Notices of the Royal Astronomical Society* 474.3 (Nov. 2017), pp. 3976–3996. ISSN: 1365-2966. DOI: [10.1093/mnras/stx3078](https://doi.org/10.1093/mnras/stx3078). URL: <http://dx.doi.org/10.1093/mnras/stx3078>.
- [13] E. P. Hubble. “Extragalactic nebulae.” In: *The Astrophysical Journal* 64 (Dec. 1926), pp. 321–369. DOI: [10.1086/143018](https://doi.org/10.1086/143018).
- [14] Federico Lelli et al. “The baryonic Tully–Fisher relation for different velocity definitions and implications for galaxy angular momentum”. In: *Monthly Notices of the Royal Astronomical Society* 484.3 (Jan. 2019), pp. 3267–3278. ISSN: 1365-2966. DOI: [10.1093/mnras/stz205](https://doi.org/10.1093/mnras/stz205). URL: <http://dx.doi.org/10.1093/mnras/stz205>.
- [15] Shengdong Lu et al. “Redshift evolution of the Fundamental Plane relation in the IllustrisTNG simulation”. In: *Monthly Notices of the Royal Astronomical Society* 492.4 (Jan. 2020), pp. 5930–5939. ISSN: 1365-2966. DOI: [10.1093/mnras/staa173](https://doi.org/10.1093/mnras/staa173). URL: <http://dx.doi.org/10.1093/mnras/staa173>.
- [16] Federico Marinacci et al. “First results from the IllustrisTNG simulations: radio haloes and magnetic fields”. In: *Monthly Notices of the Royal Astronomical Society* (Aug. 2018). ISSN: 1365-2966. DOI: [10.1093/mnras/sty2206](https://doi.org/10.1093/mnras/sty2206). URL: <http://dx.doi.org/10.1093/mnras/sty2206>.
- [17] Houjun Mo et al. *Galaxy Formation and Evolution*. 2010.
- [18] Jill P Naiman et al. “First results from the IllustrisTNG simulations: a tale of two elements – chemical evolution of magnesium and europium”. In: *Monthly Notices of the Royal Astronomical Society* 477.1 (Mar. 2018), pp. 1206–1224. ISSN: 1365-2966. DOI: [10.1093/mnras/sty618](https://doi.org/10.1093/mnras/sty618). URL: <http://dx.doi.org/10.1093/mnras/sty618>.
- [19] Julio F. Navarro et al. “The Structure of Cold Dark Matter Halos”. In: *The Astrophysical Journal* 462 (May 1996), p. 563. DOI: [10.1086/177173](https://doi.org/10.1086/177173). arXiv: [astro-ph/9508025 \[astro-ph\]](https://arxiv.org/abs/astro-ph/9508025).

- [20] Dylan Nelson et al. “First results from the IllustrisTNG simulations: the galaxy colour bimodality”. In: *Monthly Notices of the Royal Astronomical Society* 475.1 (Nov. 2017), pp. 624–647. ISSN: 1365-2966. DOI: [10.1093/mnras/stx3040](https://doi.org/10.1093/mnras/stx3040). URL: <http://dx.doi.org/10.1093/mnras/stx3040>.
- [21] Annalisa Pillepich et al. “First results from the IllustrisTNG simulations: the stellar mass content of groups and clusters of galaxies”. In: *Monthly Notices of the Royal Astronomical Society* 475.1 (Dec. 2017), pp. 648–675. ISSN: 1365-2966. DOI: [10.1093/mnras/stx3112](https://doi.org/10.1093/mnras/stx3112). URL: <http://dx.doi.org/10.1093/mnras/stx3112>.
- [22] Planck Collaboration et al. “Planck 2015 results. XIII. Cosmological parameters”. In: *The Astrophysical Journal* 594, A13 (Sept. 2016), A13. DOI: [10.1051/0004-6361/201525830](https://doi.org/10.1051/0004-6361/201525830). arXiv: [1502.01589](https://arxiv.org/abs/1502.01589) [[astro-ph.CO](#)].
- [23] William H. Press and Schechter. “Formation of Galaxies and Clusters of Galaxies by Self-Similar Gravitational Condensation”. In: *The Astrophysical Journal* 187 (Feb. 1974), pp. 425–438. DOI: [10.1086/152650](https://doi.org/10.1086/152650).
- [24] Jesse van de Sande et al. “The SAMI Galaxy Survey: comparing 3D spectroscopic observations with galaxies from cosmological hydrodynamical simulations”. In: *Monthly Notices of the Royal Astronomical Society* 484.1 (Dec. 2018), pp. 869–891. ISSN: 1365-2966. DOI: [10.1093/mnras/sty3506](https://doi.org/10.1093/mnras/sty3506). URL: <http://dx.doi.org/10.1093/mnras/sty3506>.
- [25] P. Schechter. “An analytic expression for the luminosity function for galaxies.” In: *The Astrophysical Journal* 203 (Jan. 1976), pp. 297–306. DOI: [10.1086/154079](https://doi.org/10.1086/154079).
- [26] Nicholas Scott et al. “The SAMI Galaxy Survey: Data Release Two with absorption-line physics value-added products”. In: *Monthly Notices of the Royal Astronomical Society* 481.2 (Aug. 2018), pp. 2299–2319. ISSN: 1365-2966. DOI: [10.1093/mnras/sty2355](https://doi.org/10.1093/mnras/sty2355). URL: <http://dx.doi.org/10.1093/mnras/sty2355>.
- [27] Volker Springel et al. “First results from the IllustrisTNG simulations: matter and galaxy clustering”. In: *Monthly Notices of the Royal Astronomical Society* 475.1 (Dec. 2017), pp. 676–698. ISSN: 1365-2966. DOI: [10.1093/mnras/stx3304](https://doi.org/10.1093/mnras/stx3304). URL: <http://dx.doi.org/10.1093/mnras/stx3304>.
- [28] Edward N. Taylor et al. “Galaxy And Mass Assembly (GAMA): stellar mass estimates”. In: *Monthly Notices of the Royal Astronomical Society*

- 418.3 (Dec. 2011), pp. 1587–1620. DOI: [10.1111/j.1365-2966.2011.19536.x](https://doi.org/10.1111/j.1365-2966.2011.19536.x). arXiv: [1108.0635 \[astro-ph.CO\]](https://arxiv.org/abs/1108.0635).
- [29] Jeremy Tinker et al. “Toward a Halo Mass Function for Precision Cosmology: The Limits of Universality”. In: *The Astrophysical Journal* 688.2 (Dec. 2008), pp. 709–728. DOI: [10.1086/591439](https://doi.org/10.1086/591439). arXiv: [0803.2706 \[astro-ph\]](https://arxiv.org/abs/0803.2706).
- [30] R. B. Tully and J. R. Fisher. “Reprint of 1977A&A....54..661T. A new method of determining distance to galaxies.” In: *The Astrophysical Journal* 500 (Feb. 1977), pp. 105–117.
- [31] Rainer Weinberger et al. “Simulating galaxy formation with black hole driven thermal and kinetic feedback”. In: *Monthly Notices of the Royal Astronomical Society* 465.3 (Nov. 2016), pp. 3291–3308. ISSN: 1365-2966. DOI: [10.1093/mnras/stw2944](https://doi.org/10.1093/mnras/stw2944). URL: <http://dx.doi.org/10.1093/mnras/stw2944>.
- [32] Joe Wolf et al. “Accurate masses for dispersion-supported galaxies”. In: *Monthly Notices of the Royal Astronomical Society* 406.2 (Aug. 2010), pp. 1220–1237. DOI: [10.1111/j.1365-2966.2010.16753.x](https://doi.org/10.1111/j.1365-2966.2010.16753.x). arXiv: [0908.2995 \[astro-ph.CO\]](https://arxiv.org/abs/0908.2995).
- [33] Lorenzo Zanisi et al. “Galaxy sizes and the galaxy–halo connection – I. The remarkable tightness of the size distributions”. In: *Monthly Notices of the Royal Astronomical Society* 492.2 (Dec. 2019), pp. 1671–1690. ISSN: 1365-2966. DOI: [10.1093/mnras/stz3516](https://doi.org/10.1093/mnras/stz3516). URL: <http://dx.doi.org/10.1093/mnras/stz3516>.
- [34] A V Zasov et al. “Dark matter in galaxies”. In: *Physics-Uspekhi* 60.1 (Jan. 2017), pp. 3–39. ISSN: 1468-4780. DOI: [10.3367/ufne.2016.03.037751](https://doi.org/10.3367/ufne.2016.03.037751). URL: <http://dx.doi.org/10.3367/UFNe.2016.03.037751>.